Graphene-Based Material for Microstrip Bandpass Filter

Nur I. Z. Azman[1], Nur A. A. Zaini[1], You K. Yeow[2], Fahmiruddin Esa[3], Rodziah Nazlan[1], and Mohamad A. Jusoh[1, *]

Abstract—Graphene has become one of the most essential materials in recent years due to its numerous advantages and benefits. Because of its features, graphene is becoming more widespread in a variety of applications, particularly in electrical devices. In this research, graphene thick film paste (GTP) has been used to fabricate a microstrip bandpass filter (BPF). To obtain graphene nanoparticle powder, graphene oxide (GO) was synthesized from nanoparticle graphite using the Improved Hummers Method (IHM). The graphene oxide (GO) was chemically reduced to reduced graphene oxide or graphene (rGO) using ascorbic acid as the reducing agent. The structural and morphological properties of three nanoparticle powders, G, GO, and rGO, were investigated. An X-ray Diffractometer (XRD) (Rigaku Miniflex) with a diffraction angle of $10°$ to $60°$ was used to differentiate and determine the structure of crystalline materials. Thermal stability of the samples was identified using thermogravimetric analysis (TGA). The synthesized rGO has been used to fabricate BPF circuit. The obtained nanoparticle rGO was mixed with an organic carrier composed of linseed oil, m-xylene, and α-terpineol to form GTP. The GTP was screen printed on RT duroid 5880 substrates to form BPF circuit. The BPF circuit that was created was tested for paste-to-substrate adhesion. Then, the fabricated BPF circuit was tested using vector network analyzer (VNA) and compared with conventional BPF to obtain scattering parameter results which include return loss, insertion loss, and bandwidth. The graphene BPF circuit demonstrated a good performance with return loss and insertion loss at $-27.481\,\mathrm{dB}$ and $-0.725\,\mathrm{dB}$, respectively, and a bandwidth of $1.5916\,\mathrm{GHz}$ while conventional return loss was $-26.750\,\mathrm{dB}$ and insertion loss value the same as graphene which is $-0.725\,\mathrm{dB}$ and bandwidth $0.7077\,\mathrm{GHz}$. From the result graphene BPF showed better result than conventional BPF.

1. INTRODUCTION

The increase of various technologies rapidly requires a lot of electronic devices that capable to fulfill the technology requirement such as communication technology. The demand for a range of communication services, as well as the development of technology that supports high-speed data transfer and heavier capacity, is growing as the number of communication service users increases [1]. The development of a microwave bandpass filter that has broad-bandwidth and low loss is a hot topic in research for selecting good quality signals in microwave communication systems and radio frequency (RF). A band pass filter is a device that enables frequencies within a specified frequency range to pass through while rejecting (attenuating) frequencies outside that range. Filtering of transmitted and received signals at a given centre frequency and bandwidth is required.

In microwave circuits and wireless communication systems, a microwave bandpass filter is used to achieve a unique and accurate radiation frequency [2]. Several publications have been on microwave circuits with high performance and low cost, such as antennas, filters, phase shifters, multiplexers,

couplers, and delay lines [3]. For microwave broadcasting, bandpass filters with a wide bandwidth, small size, low power consumption, and cheap cost are desired [4]. The materials to fabricate the bandpass filter also play an important rule in the performance of the circuit. Many bandpass filters have been fabricated using different types of material such as copper [1], superconductor [5], silver [6, 7], and graphene [8].

Graphene has attracted the attention of researchers because of its excellent and surprising properties. Graphene is the thinnest two-dimensional layer of carbon atoms in which the carbon atoms are arranged in a honeycomb lattice [9]. Graphene is included in carbon allotrope that contains an atomically thin two-dimensional (2D) hexagonal lattice, whereas graphene also acts as an essential part in a building block for other carbon allotropes such as zero-dimensional (0D) carbon fullerenes, one dimensional (1D) carbon nanotubes, and three-dimensional (3D) graphite [10]. There are various applications that have been developed using graphene as their main material. Graphene application has been used in technological fields, such as supercapacitor, field-effect transistors (FETs), organic photovoltaics (OPVs), light-emitting diodes (LEDs), thermal conduction, stretchable transistors, and sensor [11].

In recent years, the preparation of large-scale graphene with various advances has been made, which make graphene useful in the application of low terahertz range and microwave. Due to tunable resistivity characteristic of graphene, graphene has been utilized in RF graphene field effect transistor, graphene antenna, and graphene microstrip attenuator [8]. For instance, two tunable microstrip filters [12, 13], attenuators [14–16], and antenna [17] are proposed. Besides, a study has been proposed [18] using graphene combined with microstrip line by locating graphene in the middle of microstrip line and implementing a microwave low-pass filter by replacing metal plates with graphene [18]. Decreasing size and improves the devices performances.

In this paper, microstrip bandpass filter-based graphene is proposed to improve the performance of the circuit. The characteristics of graphene such as high conductivity because of its great charge of mobility [19], very high sensitivity and thermoelectric current effect, light weight, environmentally friendly, corrosion-resistant, mechanically stable [20], ultimate thinness [10], excellent mechanical strength, low density, thermal expansion coefficient [21], and high tensile strength which is 200 times stronger than steel [22] make graphene one of the best based materials for the fabrication of BPF.

2. MATERIALS

Graphite (C, MW $= 12.011$ g/mol), (potassium permanganate ($KMnO_4$), MW $= 158.034$ g/mol), sulfuric acid (H_2SO_4, MW $= 98.079$ g/mol), phosphoric acid (H_3PO_4, MW $= 97.994$ g/mol), potassium permanganate ($KMnO_4$), MW $= 158.034$ g/mol), 35% hydrogen peroxide (H_2O_2, MW $= 34.0147$ g/mol), ascorbic acid ($HC_6H_7O_6$, MW $= 176.12$ g/mol), m-xylene ($C_6H_4(CH_3)_2$, MW $= 106.16$ g/mol) and α-terpineol ($C_{10}H_{18}O$, MW $= 154.25$ g/mol) and linseed oil.

3. SAMPLE PREPARATION

Graphene oxide (GO) was prepared using the Improved Hummer method (IHM). A mixture of 30 ml sulfuric acid (H_2SO_4), 3.3 ml phosphoric acid (H_3PO_4), 1 g of graphite (G), and 6 g of potassium permanganate ($KMnO_4$) in a 500 ml conical flask was stirred in an ice bath. The mixture was heated at 40°C and stirred for 12 hours. Then, 100 ml of distilled water and 2 ml of 35% hydrogen peroxide (H_2O_2) were added to the mixture to form GO solution. The solutionwas then centrifuged at 10000 rpm for 15 minutes. The slurry was settled down at the bottom of the centrifuged bottle. The supernatant was removed, and the remaining solid was added with 100 ml of distilled water. This procedure was repeated until pH 5 was achieved. After achieving pH 5, the final solid as a slurry was dried in oven for 24 hours at 40°C to obtain solid GO. As shown in Figure 1, the reduction of GO to rGO was done using ascorbic acid.

The GO solution from previous synthesis was added with 0.1 M of ascorbic acid with a volume ratio of 1 : 1. The mixture was heated at 70°C on the hot plate for 30 minutes. The product was centrifuged at 12000 rpm for 10 minutes. The supernatant from the reaction decayed away, which produces solid rGO or graphene. The remaining solid rGO was washed with ethanol and water three times. The solid
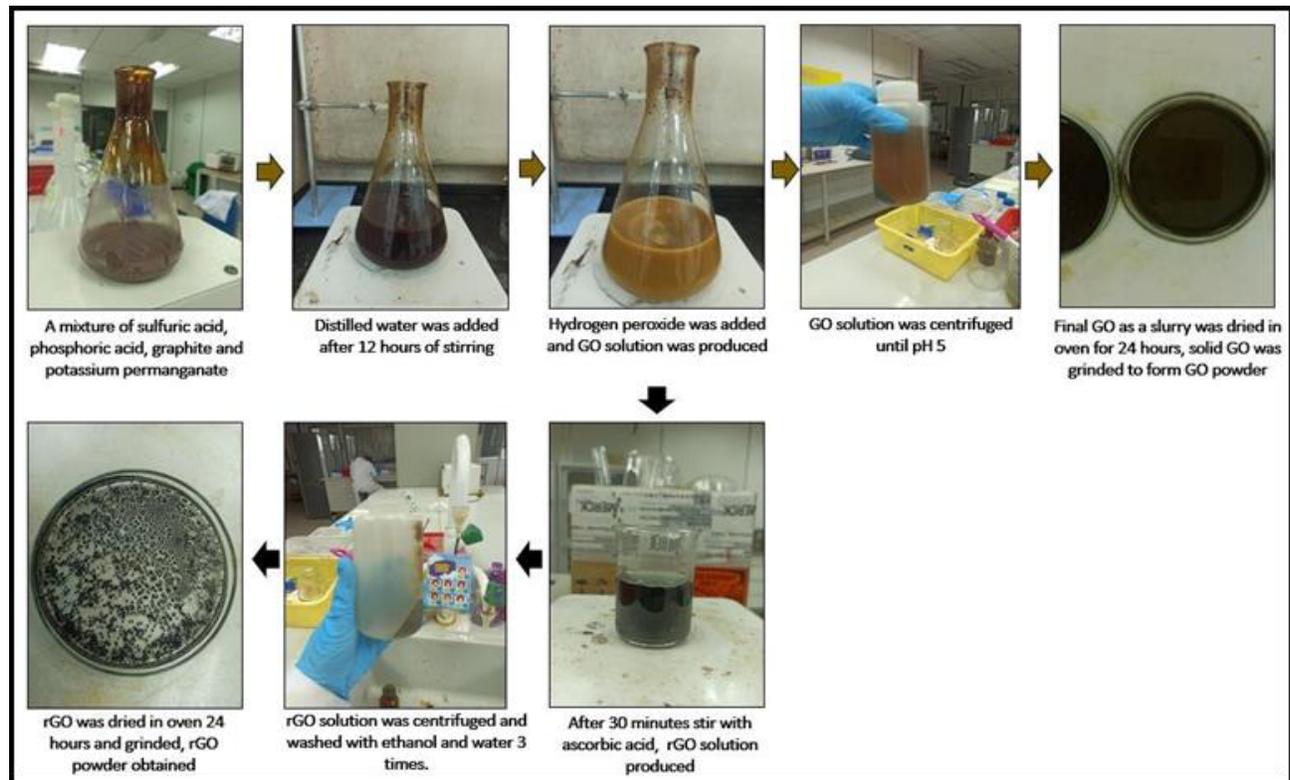
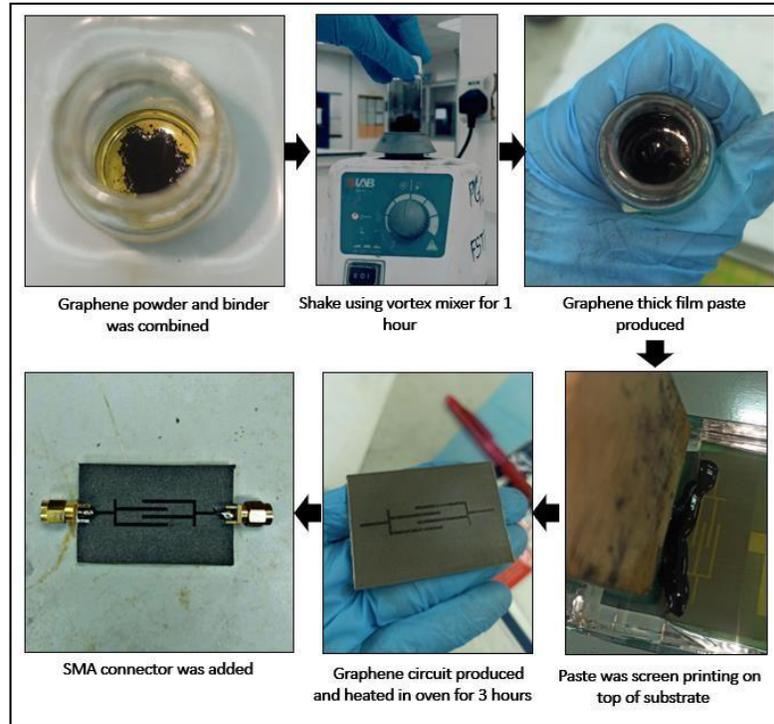**Figure 1.** Graphical representation of GO and rGO synthesis.

rGO was dried at $40°C$ in the oven for 24 hours. The rGO was ground for 2 hours to form an rGO powder.

4. CIRCUIT FABRICATION

Figure 2 shows the fabrication process of graphene BPF circuit. Firstly, the binder was prepared by combining linseed oil, m-xylene, and α-terpineol with weight percentage of 85 wt%, 12.5 wt%, and 2.5 wt%, respectively. The mixture was stirred for 2 hours at $40°C$. The binder was mixed with rGO powder by powder and binder ratio, $30:70$. The paste was shaken for 1 hour by using vortex mixer to form homogeneous paste. The produced graphene thick film paste was screen printing on top of RT duroid 5880 substrates ($\varepsilon_r = 2.2$, thickness $h = 1.57\,mm$) to form a BPF circuit. Then, the circuit was dried for 30 minutes at $80°C$ and then sintered at $300°C$ for 3 hours in an oven. The BPF circuit was leave at room temperature for 24 hours. The graphene BPF circuit was installed with SMA connector to measure the performance of the circuit.

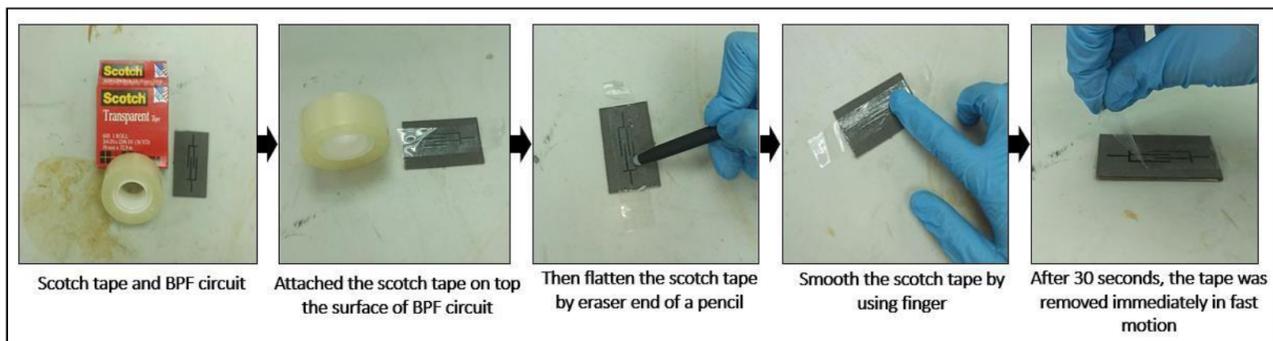## 5. STRUCTURAL AND MORPHOLOGICAL CHARACTERIZATION

The lattice parameter, crystalline size, phase, and d-spacing of the sample were determined by X-Ray diffractometer (XRD). Then, FTIR was utilized to classify the existence of every functional group in a molecule of sample, thermal stability of the graphite (G), graphene oxide (GO), and reduced graphene oxide or graphene (rGO) was determined by using thermogravimetric analysis (TGA). Field Emission Scanning Electron Microscope (FESEM) was used to obtain a high magnification picture of the material and to analyze its morphology.

Figure 2. Graphical representation of graphene BPF circuit fabrication.

6. CIRCUIT TESTING

The adhesion between the paste and substrate was justified by using a peel-off test as shown in Figure 3. The performance of the graphene BPF circuit was measured using a Vector Network Analyzer (VNA), and the results were compared with conventional BPF circuit in terms of insertion loss, return loss, and bandwidth.

Figure 3. Graphical representation of adhesion test of graphene paste on RT5880 substrate.

7. STRUCTURAL AND MORPHOLOGICAL ANALYSIS

Figure 4 shows that the interlayer distances of graphite (G), graphene oxide (GO), and reduced graphene oxide (rGO) were confirmed using X-ray diffraction (XRD) patterns. The XRD patterns of the G, GO, and rGO are shown in the figure, and the distinct and sharp peaks are produced (JCPDS file no. 75-2078), which indicate the crystalline structure of all heat-treated materials.

The 2-theta peak of graphite powder was at 26.74 deg, indicating that the interlayer distance of graphite powder was 3.36 Å. With chemical oxidation, the 2-theta peak shifted to 9.42 deg, which indicates that the graphite was fully oxidized into GO with an interlayer distance of 8.33 Å. In contrast to the XRD pattern of the rGO powder sample, the XRD pattern of the rGO yielded only a new narrow peak at 26.70 deg, indicating that the rGO was fully reduced. The interlayer distance of rGO is 3.70 Å. The narrower interlayer distance in rGO was due to the well-ordered two-dimensional structure of rGO sheets [23, 24].

The FTIR spectra of G, GO, and rGO are shown in Figure 5. A broad band is at $3351.90\,cm^{-1}$, $3435.92\,cm^{-1}$, and $3455.56\,cm^{-1}$ which belongs to a strong stretching mode of OH group, and an absorption peak is at $1638.40\,cm^{-1}$, $1633.13\,cm^{-1}$, and $1640.96\,cm^{-1}$ due to C $=$ C stretching mode. In GO, the peaks are at $1739.80\,cm^{-1}$, $1385.8\,cm^{-1}$, $1079.49\,cm^{-1}$, and $542.0\,cm^{-1}$ which correspond to the stretching modes of C $=$ O, C-H, C-OH, and C-O, respectively. However, for rGO and G, the absorption peaks at $1739.80\,cm^{-1}$, $1385.80\,cm^{-1}$, and $1079.49\,cm^{-1}$ were reduced. These results indicate that the partial functional groups in GO had been effectively eliminated during reduction [25, 26], and these peaks did not appear in the spectrum of graphite indicating that the oxidation steps have introduced strong oxygen containing functional groups in GO [27]. rGO is similar to the graphite, which indicates the restoration of electronic conjugation within the graphene sheets [28]. When the intensity of these peaks in GO decreases in rGO, it shows the removal of oxygen containing functional groups to a certain degree [29].

Thermal degradation or stability of the graphite (G), graphene oxide (GO), and reduced graphene oxide (rGO) was investigated by thermogravimetric analysis (TGA). The reaction progress during the thermal reduction of the graphite, GO, and rGO was monitored by TGA in the range 30°C to 600°C under nitrogen atmosphere at $10°C\,min^{-1}$ heating rates. Figure 6 presents three different graphs for G, GO, and rGO. It clearly shows that graphite (G) has a slight weight loss and is thermally stable at 600°C, while GO is thermally decomposed into three steps. A huge weight loss happened at 100°C because of the hydrophilic nature of GO which removed the adsorbed water molecules. At 200°C, there was a significant weight loss, because oxygen accommodate functional groups present on the GO surface were decomposed. Next, at 300°C there was a notable weight loss because more stable oxygen held in functional groups to CO and CO_2 was decomposed [24]. From Figure 6, the rGO graph indicates a very small weight loss (28%) compared to GO (87%) along the temperature range (30°C to 600°C), and in spite of that, rGO shows bigger weight loss than graphite which is 12%, illustrating that graphite has
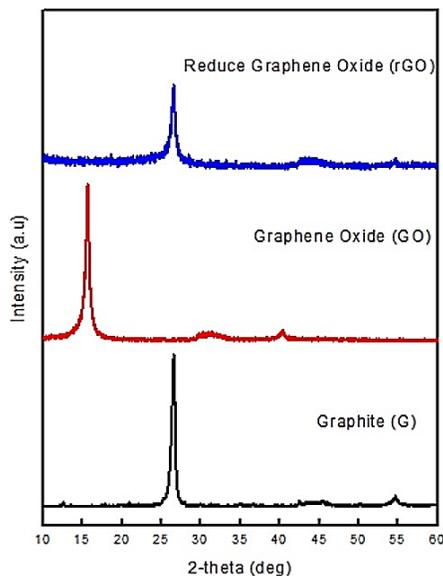
**Figure 4.** XRD patterns of graphite (G), graphene oxide (GO) and graphene (rGO).
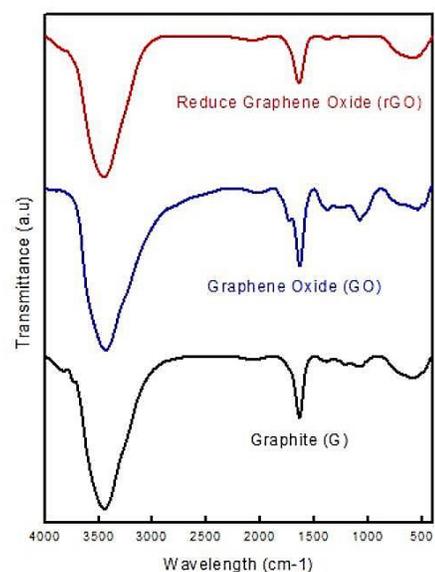
Figure 5. FTIR spectra of G, GO and rGO powder.
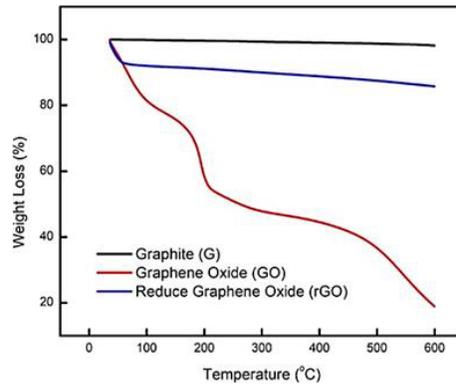
Figure 6. TGA result for G, GO and rGO powder.

lower oxygenated functional groups than rGO. However, the fraction of oxygen containing functional groups in GO is bigger than rGO [23].

The morphologies of graphite (G), graphene oxide (GO), and reduced graphene oxide (rGO) were presented in Figures 7(a)–(c). It can be clearly seen that the morphology of GO is more loose than G and rGO because surface modification treatment has resulted in tiny wrinkles over the graphene sheets of graphene oxide. Because of reduction by using ascorbic acid, rGO agglomeration is formed as a result of the oxygenic groups on the GO surface being removed leading to a decrease in the distance between layers of the GO [30]. Besides, the exfoliation process resulted in rGO with wrinkled and fluffy morphology [31].
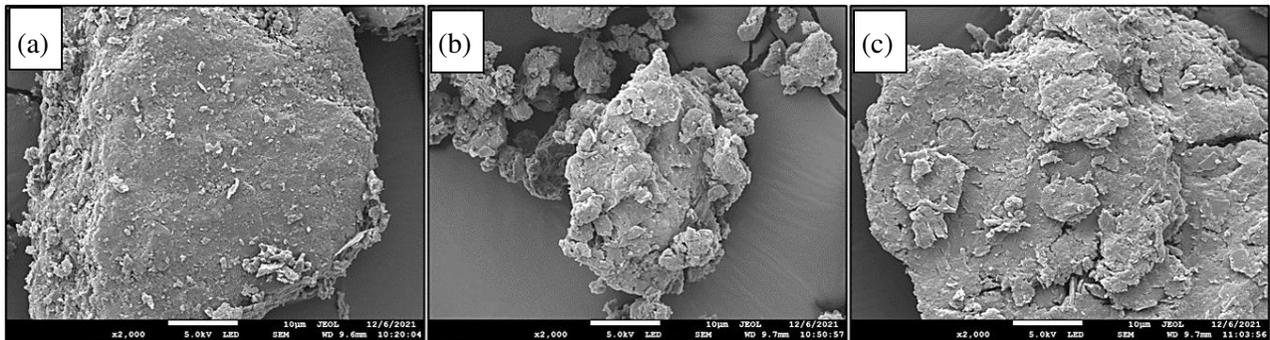

Figure 7. FESEM of (a) graphite, (b) graphene oxide and (c) reduced graphene oxide at 2000x magnification.

8. CIRCUIT TESTING AND PERFORMANCE

The observation for the adhesion test showed that the scotch tape was completely clean after peeling off from the circuit which showed strong adhesion between the paste and substrate resulting in good preparation and fabrication of the circuit.

8.1. Return Loss

Return loss occurs because of mismatches between the transmission line and feeding points. It displays the value of feeding power reflected back at the microstrip filter's port. Reflections at the port reflect back towards the source when the microstrip and transmission line are not exactly matched, resulting in a standing wave. The BPF radiates optimally at the specified resonance frequency of 5 GHz. Figure 8
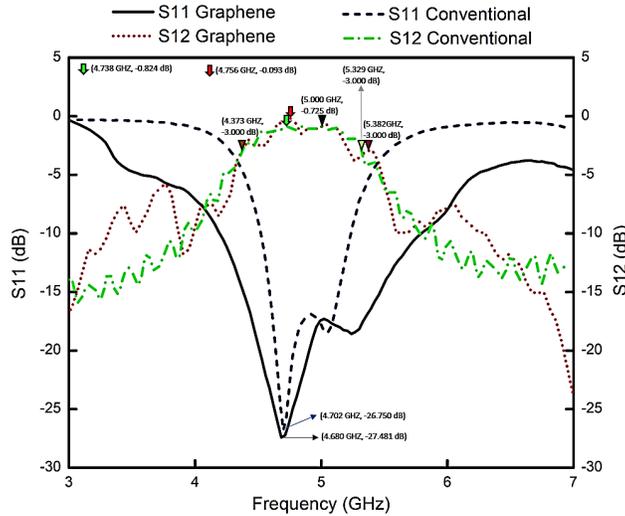
Figure 8. Return loss (S_{11}) and insertion loss (S_{12}) of graphene and conventional BPF circuit.

shows a return loss of graphene BPF and conventional BPF circuit at frequencies of 3 GHz and 7 GHz. It can be clearly seen that the highest return loss of graphene BPF is -27.481 dB at operating frequency of 4.680 GHz, and the highest return loss of conventional BPF is -26.750 dB at operating frequency of 4.750 GHz. Both circuits show a good performance which have return loss value greater than -20 dB as the typical filter should have a high amount of return loss for better performance [2].

8.2. Insertion Loss

The insertion losses of graphene and conventional BPF are shown in Figure 8. It can be clearly seen that the minimum insertion losses of graphene and conventional BPF are -0.093 dB (4.756 GHz) and -0.824 dB (4.738 GHz), respectively, found at operating frequency of 5 GHz. From Figure 8 it can be observed that S_{12} for graphene and conventional BPFs at frequency 5 GHz are -0.725 dB which is almost close to zero insertion losses. The operation frequency of graphene BPF is 4.373–5.382 GHz while conventional BPF is 4.373–5.329 GHz. As mentioned by [2], a typical filter should have a high amount of lower insertion indicating a good result of insertion loss for graphene BPF.

8.3. Bandwidth

The bandwidth of a microstrip bandpass filter is the range of frequencies over which it can function properly. The number of frequencies (GHz) for which the standing wave ratio is less than 2:1 is the filter's bandwidth [32]. The center frequency and 6 dB fractional bandwidth (FBW) were calculated for both circuits. It was found that the graphene BPF showed a higher center frequency at 4.9855 GHz than the conventional BPF at 4.8865 GHz. Meanwhile, the 6 dB FBW of graphene BPF is also higher as 46.11% was calculated for graphene BPF and 18.81% for conventional BPF. From the value obtained, the center frequency for graphene is higher than the conventional one, and the frequency bandwidth for graphene also shows a bigger value than conventional one. Besides, the graph return loss against frequency at point -10 dB can be used to determine the value of bandwidth. The bandwidths of graphene and conventional BPF were 1.5916 GHz and 0.7077 GHz, respectively. From the value, graphene has bigger bandwidth than conventional one which indicates better performance for graphene BPF.

Figure 9(a) shows the 2D radiation pattern and gain results of graphene BPF. The simulation radiation pattern of graphene-based bypass filter integrating at 5 GHz in H-plane and E-plane is illustrated in the figure. Figure 9(b) shows the 3D radiation pattern of fabricated bypass filter. Figure 9(c) illustrates the surface current distribution of bandpass filter elements at 5 GHz.
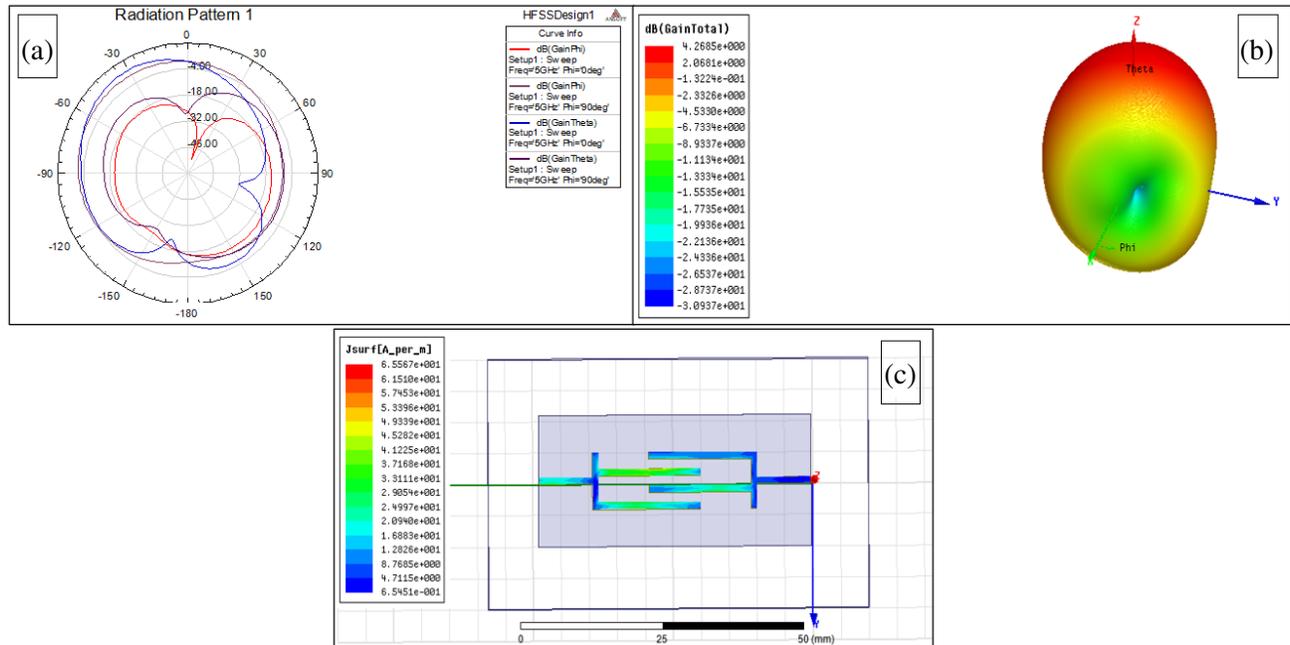
Figure 9. Electric and magnetic field distribution of the graphene BPF (a) 2D radiation pattern, (b) 3D radiation pattern, and (c) electromagnetic field distribution.

From the analysis result of circuit performances which include return loss, insertion loss, and bandwidth, graphene-based bandpass filter has shown a great result compared to conventional bandpass filter. The graphene BPF circuit demonstrated a good performance with return loss (-27.481 dB) compared to conventional BPF (-26.750 dB). Next, the insertion loss shows the same value for graphene BPF which was -0.725 dB and conventional BPF also -0.725 dB while the bandwidth for graphene BPF was 1.5916 GHz, and that of conventional BPF was 0.7077 GHz. The different return loss and bandwidth values for graphene and conventional BPF show that the proposed BPF, which is graphene, has good performances and better result than conventional BPF.

9. CONCLUSIONS

This paper presents graphene oxide successfully synthesized using an improved hummer method. The structural and morphological properties of G, GO, and rGO have been identified and observed. The great purity and crystallinity of samples were confirmed using XRD. The functional group of the materials was successfully obtained using FTIR. Thermal stability has been identified and determined, and the morphology has been observed.

The graphene microstrip bandpass filter (BPF) has an operating frequency of 4.373–5.382 GHz with transmission frequencies in the range of 3–7 GHz, 4.9855 GHz of center frequency, return loss of -27.481 dB, insertion loss of -0.725 dB, and bandwidth of ~ 1.59 GHz, showing a better result as than conventional BPF.

REFERENCES

1. Juanda, E. A., T. Hariyadi, U. Mukhidin, and R. N. Yuniar, "Design and development of band pass filter microstrip cascade trisection with open stub and defected ground structure (DGS) in 1800 MHz frequency," *Journal of Engineering Science and Technology (JESTEC)*, Vol. 15, No. 1, 372–381, 2020, jestec.taylors.edu.my/Vol%2015%20issue%201%20February%202020/15_1_28.pdf.

2. Jasim, S. E., M. A. Jusoh, S. N. S. Mahmud, and A. H. Zamani, "Design of 2.5 GHz broad bandwidth microwave bandpass filter at operating frequency of 10 GHz using HFSS," *IOP Conference Series: Materials Science and Engineering*, Vol. 342, No. 1, 012022, IOP Publishing, April 2018, dx.doi.org/10.1088/1757-899X/342/1/012022.

3. Newman, N. and W. G. Lyons, "High-temperature superconducting microwave devices: Fundamental issues in materials, physics, and engineering," *Journal of Superconductivity*, Vol. 6, No. 3, 119–160, 1993, doi.org/10.1007/BF00625741.

4. Liu, A. Q., A. B. Yu, and Q. X. Zhang, "Broad-band band-pass and band-stop filters with sharp cut-off frequencies based on series CPW stubs," *2006 IEEE MTT-S International Microwave Symposium Digest*, 353–356, IEEE, June 2006, doi.10.1109/MWSYM.2006.249525.

5. Nisenoff, M., "Microwave superconductivity Part 1: History, properties and early applications," *2011 IEEE MTT-S International Microwave Symposium*, 1–4, IEEE, June 2011, doi.10.1109/MWSYM.2011.5972594.

6. Vineetha, K. V., M. S. Kumar, B. T. P. Madhav, and M. C. Rao, "Flexible bandpass filter with silver conductive layer for GPS, ISM, PCS, LTE and WLAN applications," *Materials Today: Proceedings*, Vol. 42, 1321–1328, 2021, doi.org/10.1016/j.matpr.2020.12.1187.

7. Ahmad, W., D. Budimir, A. Maric, and N. Ivanisevic, "Inkjet printed bandpass filters and filtennas using silver nanoparticle ink on flexible substrate," *2015 IEEE International Symposium on Antennas and Propagation & USNC/URSI National Radio Science Meeting*, 145–146, IEEE, July 2015, doi.10.1109/APS.2015.7304458.

8. Chen, J., J. Zhang, Y. Zhao, L. Li, T. Su, C. Fan, and B. Wu, "High-selectivity bandpass filter with controllable attenuation based on graphene nanoplates," *Materials*, Vol. 15, No. 5, 1694, 2022, doi.org/10.3390/ma15051694.

9. Sa'don, S. N. H., M. H. Jamaluddin, M. R. Kamarudin, F. Ahmad, Y. Yamada, K. Kamardin, and I. H. Idris, "Analysis of graphene antenna properties for 5G applications," *Sensors*, Vol. 19, No. 22, 4835, 2019, doi.org/10.3390/s19224835.

10. Lee, H. J. and J. G. Yook, "Graphene nanomaterials-based radio-frequency/microwave biosensors for biomaterials detection," *Materials*, Vol. 12, No. 6, 952, 2019, doi.org/10.3390/ma12060952.

11. Fowler, J. D., M. J. Allen, V. C. Tung, Y. Yang, R. B. Kaner, and B. H. Weiller, "Practical chemical sensors from chemically derived graphene," *ACS Nano*, Vol. 3, No. 2, 301–306, 2009, doi.org/10.1021/nn800593m.

12. Zhang, A. Q., W. B. Lu, Z. G. Liu, H. Chen, and B. H. Huang, "Dynamically tunable substrate-integrated-waveguide attenuator using graphene," *IEEE Transactions on Microwave Theory and Techniques*, Vol. 66, No. 6, 3081–3089, 2018, doi.10.1109/TMTT.2018.2809577.

13. Ilić, A. Ž., B. M. Bukvić, D. Budimir, and M. M. Ilić, "Tuning the filter responses with graphene based resonators," *2019 International Conference on Electromagnetics in Advanced Applications (ICEAA)*, 0151–0152, IEEE, September 2019, doi.10.1109/ICEAA.2019.8879418.

14. Pierantoni, L., D. Mencarelli, M. Bozzi, R. Moro, S. Moscato, L. Perregrini, and S. Bellucci, "Broadband microwave attenuator based on few layer graphene flakes," *IEEE Transactions on Microwave Theory and Techniques*, Vol. 63, No. 8, 2491–2497, 2015, doi.10.1109/TMTT.2015.2441062.

15. Yasir, M., S. Bistarelli, A. Cataldo, M. Bozzi, L. Perregrini, and S. Bellucci, "Enhanced tunable microstrip attenuator based on few layer graphene flakes," *IEEE Microwave and Wireless Components Letters*, Vol. 27, No. 4, 332–334, 2017, doi.10.1109/LMWC.2017.2679042.

16. Wu, B., C. Fan, X. Feng, Y. T. Zhao, J. Ning, D. Wang, and T. Su, "Dynamically tunable filtering attenuator based on graphene integrated microstrip resonators," *IEEE Transactions on Microwave Theory and Techniques*, Vol. 68, No. 12, 5270–5278, 2020, doi.10.1109/TMTT.2020.3017197.

17. Yasir, M., P. Savi, S. Bistarelli, A. Cataldo, M. Bozzi, L. Perregrini, and S. Bellucci, "A planar antenna with voltage-controlled frequency tuning based on few-layer graphene," *IEEE Antennas and Wireless Propagation Letters*, Vol. 16, 2380–2383, 2017, doi.10.1109/LAWP.2017.2718668.

18. Wu, B., Y. Zhang, H. Zu, C. Fan, and W. Lu, "Tunable grounded coplanar waveguide attenuator based on graphene nanoplatesm," *IEEE Microwave and Wireless Components Letters*, Vol. 29, No. 5, 330–332, 2019, doi.10.1109/LMWC.2019.2908034.

19. Wang, W., C. Ma, X. Zhang, J. Shen, N. Hanagata, J. Huangfu, and M. Xu, "High-performance printable 2.4 GHz graphene-based antenna using water-transferring technology," *Science and Technology of Advanced Materials*, Vol. 20, No. 1, 870–875, 2019, doi.org/10.1080/14686996.2019.1653741.

20. Song, R., G. L. Huang, C. Liu, N. Zhang, J. Zhang, C. Liu, and D. He, "High-conductive graphene film based antenna array for 5G mobile communications," *International Journal of RF and Microwave Computer-Aided Engineering*, Vol. 29, No. 6, e21692, 2019, doi.org/10.1002/mmce.21692.

21. Hsieh, C. C. and W. R. Liu, "Synthesis and characterization of nitrogen-doped graphene nanosheets/copper composite film for thermal dissipation," *Carbon*, Vol. 118, 1–7, 2017, doi.org/10.1016/j.carbon.2017.03.025.

22. Andrijanto, E., S. Shoelarta, G. Subiyanto, and S. Rifki, "Facile synthesis of graphene from graphite using ascorbic acid as reducing agent," *AIP Conference Proceedings*, Vol. 1725, No. 1, 020003, AIP Publishing LLC, April 2016, doi.org/10.1063/1.4945457.

23. Soltani, T. and B. K. Lee, "A benign ultrasonic route to reduced graphene oxide from pristine graphite," *Journal of Colloid and Interface Science*, Vol. 486, 337–343, 2017, doi.org/10.1016/j.jcis.2016.09.075.

24. El Achaby, M., F. Z. Arrakhiz, S. Vaudreuil, E. M. Essassi, and A. Qaiss, "Piezoelectric β-polymorph formation and properties enhancement in graphene oxide-PVDF nanocomposite films," *Applied Surface Science*, Vol. 258, No. 19, 7668–7677, 2012, doi.org/10.1016/j.apsusc.2012.04.118.

25. Gong, Y., D. Li, Q. Fu, and C. Pan, "Influence of graphene microstructures on electrochemical performance for supercapacitors," *Progress in Natural Science: Materials International*, Vol. 25, No. 5, 379–385, 2015, doi.org/10.1016/j.pnsc.2015.10.004.

26. Faniyi, I. O., O. Fasakin, B. Olofinjana, A. S. Adekunle, T. V. Oluwasusi, M. A. Eleruja, and E. O. B. Ajayi, "The comparative analyses of reduced graphene oxide (RGO) prepared via green, mild and chemical approaches," *SN Applied Sciences*, Vol. 1, No. 10, 1–7, 2019, doi.org/10.1007/s42452-019-1188-7.

27. Akhavan, O., M. Kalaee, Z. S. Alavi, S. M. A. Ghiasi, and A. Esfandiar, "Increasing the antioxidant activity of green tea polyphenols in the presence of iron for the reduction of graphene oxide," *Carbon*, Vol. 50, No. 8, 3015–3025, 2012, doi.org/10.1016/j.carbon.2012.02.087.

28. Pasricha, R., S. Gupta, A. G. Joshi, N., Bahadur, D. Haranath, K. N. Sood, and S. Singh, "Directed nanoparticle reduction on graphene," *Materials Today*, Vol. 15, No. 3, 118–125, 2012, doi.org/10.1016/S1369-7021(12)70047-0.

29. Esfandiar, A., O. Akhavan, and A. Irajizad, "Melatonin as a powerful bio-antioxidant for reduction of graphene oxide," *Journal of Materials Chemistry*, Vol. 21, No. 29, 10907–10914, 2011, doi.org/10.1039/C1JM10151J.

30. Hsieh, C. T., C. Y. Lin, Y. F. Chen, J. S. Lin, and H. Teng, "Silver nanorods attached to graphene sheets as anode materials for lithium-ion batteries," *Carbon*, Vol. 62, 109–116, 2013, doi.org/10.1016/j.carbon.2013.06.002.

31. Bhanuprakash, L., T. A. Sajith, and S. Varghese, "Study of mechanical performances of epoxy nanocomposites with exfoliated-reduced graphene oxide," www.researchgate.net/publication/333421331_Study_of_Mechanical_Performances_of_Epoxy_Nano composites_with_Exfoliated-_Reduced_Graphene_Oxide.

32. Mahmud, S. N. S., M. A. Jusoh, S. E. Jasim, A. H. Zamani, and M. H. Abdullah, "Design, simulation and analysis a microstrip antenna using PU-EFB substrate," *IOP Conference Series: Materials Science and Engineering*, Vol. 342, No. 1, 012021, IOP Publishing, April 2018, doi.10.1088/1757-899X/342/1/012021.